Studies of Standard Heat Treatment Effects on Microstructure and Mechanical Properties of Laser Net Shape Manufactured INCONEL 718

H. QI, M. AZER, and A. RITTER

Laser net shape manufacturing (LNSM) is a laser cladding/deposition based technology, which can fabricate and repair near-net-shape high-performance components directly from metal powders. Characterizing mechanical properties of the laser net shape manufactured components is prerequisite to the applications of LNSM in aircraft engine industrial productions. Nickel-based superalloys such as INCONEL 718 are the most commonly used metal materials in aircraft engine high-performance components. In this study, the laser deposition process is optimized through a set of designed experiments to reduce the porosity to less than 0.03 pct. It is found that the use of plasma rotating electrode processed (PREP) powder and a high energy input level greater than 80 J/mm are necessary conditions to minimize the porosity. Material microstructure and tensile properties of laser-deposited INCONEL 718 are studied and compared under heat treatment conditions of as deposited, direct aged, solution treatment and aging (STA), and full homogenization followed by STA. Tensile test results showed that the direct age heat treatment produces the highest tensile strength equivalent to the wrought material, which is followed by the STA-treated and the homogenization-treated tensile strengths, while the ductility exhibits the reverse trend. Finally, failure modes of the tensile specimens were analyzed with fractography.

I. INTRODUCTION

LASER net shape manufacturing (LNSM) is a laser cladding based freeform fabrication technology that uses a high energy laser beam to create three-dimensional geometries by precisely cladding thin layers of metal powder on a base material. As a rapid manufacturing method without the assistance of tooling, this technology enables quick access to new design concepts, shortens the new product introduction cycle, and enables near-net-shape repairs of costly components. One of the important applications of the LNSM technology developed at the General Electric Global Research Center is to provide an economic and flexible method to fabricate and repair high-performance components in aircraft engines, i.e., blisk blades, compressor blades, and turbine components. Geometric accuracy and material properties are the two basic, but challenging, requirements for final implementation of LNSM technology in the aircraft engine industry.

INCONEL* 718 (IN718) has been the most widely

---

*INCONEL is a trademark of Inco Alloys International, Huntington, WV.

---

used nickel-based superalloy in the aircraft engine industry over the past 40 years. It has been used in many aircraft engine components, i.e., critical rotating parts, airfoils, supporting structures, and pressure vessels, accounting for over 30 pct of the total finished component weight of a modern aircraft engine.[1,2] IN718 was designed to retain high strength, creep resistance, and good fatigue life at high temperature up to 650 °C. It can be strengthened by precipitating γ'' (Ni$_3$Nb) and γ' (Ni$_3$(Al,Ti)) phases in the γ matrix at normal volume fractions of approximately 16 and 4 pct, respectively, after a full heat treatment.[3] IN718 is known to have good weldability due to its relatively slow precipitation strengthening kinetics; however, the solidification process of cast or welded IN178 is often associated with segregation of high concentration refractory elements, such as Nb and Mo. As a result, a Nb-rich brittle intermetallic compound called Laves phase, represented as (Ni,Cr,Fe)$_2$(Nb,Mo,Ti), often forms at the interdendritic regions.[4] Laves phase is known to be detrimental to the material tensile ductility, fatigue, and creep rupture properties,[3,5,6] as it depletes the principle elements needed for precipitation strengthening and aids in easy crack initiation and propagation.

H. QI, Laser Processing Engineer, and M. AZER, Manager, Laser and Metrology Systems Laboratory, Material Systems Technologies, and A. RITTER, Principal Scientist, Ceramics and Metallurgy Technologies, are with General Electric Global Research Center, Niskayuna, NY 12309. Contact e-mail: qih@research.ge.com

Previous research showed that the morphology and composition of Laves phase depended strongly on the heat input and the cooling rate of a welding process;[7] i.e., welding processes with lower heat input and higher cooling rates produce less Laves phase, and consequently better material properties.

Previous literature has reported the tensile properties of laser-deposited IN718 (typically after solution and precipitation heat treatment) and has claimed properties equivalent or superior to the wrought properties. This is due to the fine grain size and small dendrite arm spacing as the results of the rapid solidification rate associated with laser deposition. Blackwell[8] studied the tensile properties of laser-deposited IN718 by the LENS**

**LENS is a trademark of Optomec, Albuquerque, NM.

---

system and found the deposit exhibited anisotropic properties, which are the result of a weak substrate/deposit bond or lack of bonding between successive layers of the deposit. He also found that a subsequent hot isostatic pressing treatment can significantly reduce the anisotropic ductility of the deposit, but also substantially coarsen the base material grain size. Kelbassa et al.[9] used a short aging method (732 °C for 4 hours) to heat treat the laser-deposited IN718 and achieved properties equivalent to forged tensile properties at room temperature and at 650 °C. Zhao et al.[10] compared the microstructure and mechanical properties of IN718 deposited with the gas-atomized (GA) powder and the plasma rotating electrode processed (PREP) powder. They found that the GA powder produces inferior tensile and stress rupture properties due to the existence of hollow particles in the GA powder, which cause microcracks and porosity in laser-deposited samples.

The aim of this work is to optimize the laser deposition process parameters for high-quality deposits, to evaluate the industrial standard heat treatment methods on laser-deposited IN718, and to characterize the resultant material microstructures and tensile properties of deposited IN718 for the applications of net shape manufacturing and repair of aircraft engine components. The tensile properties of the alloy in the as-deposited, direct-aged, STA-treated, and homogenization-treated conditions are compared and correlated with their corresponding microstructure features.

II. EXPERIMENTAL PROCEDURE

A LNSM system consists of a CO_2 laser, a multiaxis CNC platform, an argon environment glove box, a multihopper powder feeder, and a four-way powder delivery nozzle. Figure 1 shows the schematics of the laser powder deposition process. A 1.5 kW PRC CO_2 laser with a "D" mode (a combination of the TEM00 and TEM01* modes) beam is used in the LNSM system. This mode produces an intensity profile with a relatively flat top and steep sides compared to a
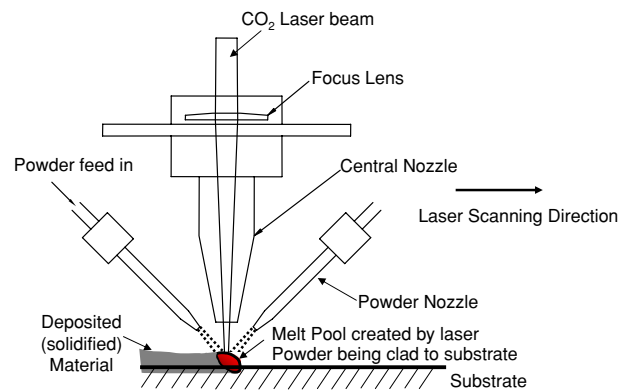

Fig. 1—Schematic of the laser powder deposition process.

Table I. Chemical Compositions of IN718 Powders (Weight Percent)

Element	GA Powder	PREP Powder
Ni	53.05	54.82
Fe	17.58	17.00
Cr	18.23	18.08
Mo	3.06	3.10
Nb + Ta	5.10	5.17
Ti	0.94	0.89
Al	0.44	0.53
Co	0.27	0.17
C	0.04	0.03
Si	0.12	0.08

Gaussian beam. The laser beam is focused by a lens with 127-mm focusing length through a central nozzle. Argon gas is supplied into the central nozzle to protect the focus lens from contamination and provide shielding to the melt pool. Four powder feed nozzles with 0.97-mm inner diameter deliver fine powder streams to the melt pool symmetrically from four directions. The powders used in this study are commercially available IN718 powder (mesh size −100/+325) manufactured by the GA and PREP methods, respectively. The chemical compositions of the GA and PREP IN718 powders used in this study are given in Table I. All the deposition experiments were conducted inside a glove box, where the concentration of oxygen was maintained below 20 ppm.

In order to manufacture the test samples with good quality and obtain the best capable mechanical property results, the following procedures were followed in this study:

(1) toolpath optimization for multipass deposition;
(2) porosity assessment;
(3) process improvement, if needed;
(4) heat treatment study;
(5) metallographic study;
(6) manufacturing of tensile test samples;
(7) machining samples; and
(8) tensile testing.

A. Process Optimization

Prior to making the samples for mechanical property tests, experimental studies were performed to investigate factors affecting the porosity levels in the laser-deposited samples, as porosities are known to deteriorate the ductility and fatigue life of the deposited material. Porosity generated in the laser deposition process is identified primarily from three sources: lack of fusion between deposition passes and layers, hollow powder particles produced during the GA or PREP process, and processing gas entrapped during deposition. Lack of fusion normally appears as irregular shapes along the fusion lines between two passes or layers and is associated with partially melted powders. The latter two porosity sources often result in circular-shaped pores. Lack-of-fusion pores can be eliminated by optimizing the laser heat input and geometric toolpath parameters, *i.e.*, bead overlap ratio and bead aspect ratio.[11] In this study, experiments were designed in order to minimize the porosity caused by hollow powders and entrapped gas bubbles. Three types of IN718 powders with different particle size distributions and manufacturing methods were investigated (as shown in Table II). Figure 2 shows the representative micrographs of these three powders. It can be observed from Figure 2 that the GA powders generally contain a certain fraction of hollow particles. The coarse GA powder contains more hollow particles and larger pores than the fine GA powder. In contrast, hardly any hollow particles can be found in the PREP powder. Laser deposition parameters, laser power, travel speed, and layer height were varied in these experiments to reveal the effect of these parameters on the resulting porosities. Table III gives the ranges of each parameter used in this study. Within the selected range of each parameter, a high level value (+1) and a low level value (−1) were selected, respectively, for the designed experiments. A set of two-level, three-factor (eight conditions) full factorial designed experiments was conducted with each type of the IN718 powder shown in Table II. This resulted in a total of 24 deposition runs. Solid rectangular blocks of 19 mm × 6 mm × 6 mm were deposited with the raster pattern toolpath. Each of the samples was sectioned at two transverse locations for examination of its internal porosities. The porosities were then measured with imaging analysis software based on the microscopic images of the sectioned surface and calculated as percentage values of the analyzed areas.

B. Porosity Results

Figure 3 shows the microscope pictures of sectioned surfaces from three samples deposited with the same set of process parameters but different IN718 powders. These samples were deposited with the same laser power 425 W (+1), speed 5 mm/s (+1), and layer height 0.127 mm (−1), which is one of the eight designed experiment conditions, but resulted in different porosity levels due to the different powder sources. The coarse GA powder produces a mean porosity of 0.75 ± 0.03 pct, the fine GA powder produces 0.51 ± 0.02 pct, and the PREP powder produces 0.03 ± 0.03 pct. To examine the effects of the process parameters, linear energy was calculated for each experiment condition, which is defined as laser power/speed (J/mm). Figure 4 shows the measured porosity values at the four different linear energy levels from the designed experiments. It is observed that the resultant porosities are inversely proportional to the linear energy. This trend is more obvious with the GA powders, where the porosities are minimized to 0.33 pct for the coarse GA powder and 0.19 pct for the fine GA powder at the highest energy input 111.5 J/mm. The PREP powder has produced

Table II. Three Types of Commercial IN718 Powders

Powder	Manufacturing Method	Mesh Size	Micron
GA coarse	gas atomized	−120/+200	74 to 125
GA fine	gas atomized	−200/+325	44 to 74
PREP	plasma rotating electrode processed	−100/+325	44 to 149

Table III. Ranges of Laser Parameters for Porosity Study

Parameters	Laser Power (W)	Travel Speed (mm/s)	Layer Height (mm)
Range	250 to 550	2.0 to 8.0	0.1 to 0.4

Coarse GA powder
Mesh size -120/+325

Fine GA Powder
Mesh size -170/+325

PREP Powder
Mesh size -100/+325

0.1mm   0.1mm   0.1mm

Fig. 2—Micrographs of the three types of IN718 powder used in this study.
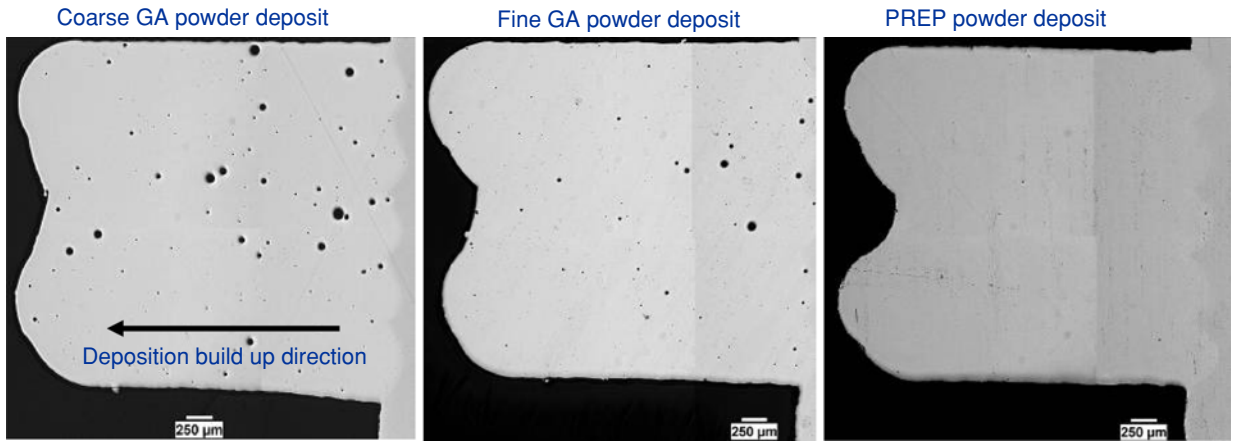
Fig. 3—Sectioned surfaces of the deposition samples fabricated with the same set of process parameters, *i.e.*, laser power 425 W (+1), speed 5 mm/s (+1), and layer height 0.127 mm (−1), but different sources of IN718 powder. Sectioned surfaces exhibit clearly different porosity levels.
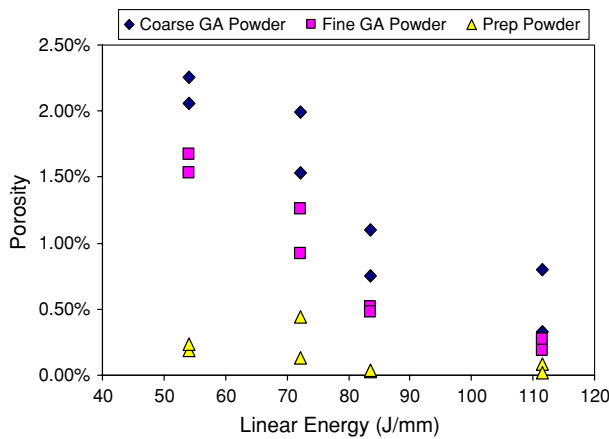

Fig. 4—Effect of the laser linear energy input (laser power/scanning speed) on the resultant porosity of each deposit. Four linear energy values are from the eight runs of the designed experiments.

Table IV. Three Heat Treatment Methods for Laser-Deposited IN718

Homogenized STA* (Steps 1 + 2 + 3)	STA** (Steps 2 + 3)	Direct Aging (Step 3)
Step 1 homogenization	heat to 1093 °C ± 14, hold for 1 to 2 h, air cool or faster	
Step 2 solution	heat to 954 to 982 °C, hold for >1 h, air cool or faster	
Step 3 aging	heat to 718 °C ± 8, hold for 8 h, furnace cool to 621 °C ± 8, hold for 10 h, air cool or faster	

*According to AMS-5383D for cast IN718.
**According to AMS-5662M for forged IN718.

significantly lower porosities compared to the GA powders. It can be seen that the porosity is reduced to less than 0.08 pct with PREP powder when the linear energy input is kept above 80 J/mm. Based on this study, all the following deposition experiments were performed with PREP IN718 powder and appropriate linear energy values for the best quality of deposition.

C. Heat Treatment and Microstructure Evaluation

Postweld heat treatment is necessary to relieve the residual stresses and enable the precipitation of strengthening phases. Microstructures from a laser deposition process are usually different from those resulting from the conventional cast and wrought processes due to the inherent rapid solidification rate associated with laser deposition. It is necessary to investigate how the industrial standard heat treatment methods (usually for cast and wrought IN718) affect the laser-deposited microstructures and eventually the mechanical properties of the material. In this study, three heat treatment

methods conforming to Aerospace Material Specifications (AMS) were evaluated for laser-deposited IN718 samples, *i.e.*, direct age, solution treatment and age (STA), and homogenization followed by STA. Table IV presents the detailed conditions for each heat treatment method used in this study. Solid rectangle samples with dimensions of 20 mm (L) × 8 mm (W) × 8 mm (H) were deposited with IN718 PREP powder and a constant 96 J/mm linear energy for these heat treatment studies. Samples were heat treated, sectioned, polished, and etched with a Kallings etchant. Microstructures at different heat treatment conditions were examined by optical microscopy and scanning electron microscopy (SEM). Energy dispersive X-ray spectroscopy (EDAX) analysis was performed for qualitative elemental characterization of featured phases based on the SEM observations.

Figure 5 demonstrates the microstructures of the transverse cross section of the as-deposited IN718 sample. Staggered individual deposit layers can be observed from the low-magnification microscopy
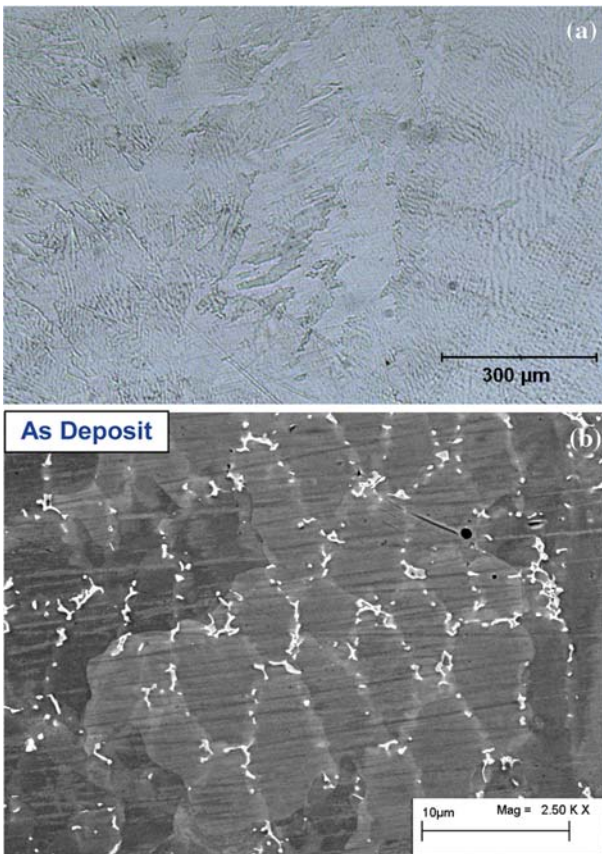
Fig. 5—Microstructure of transverse cross sections of the as-deposited IN718 sample: (a) optical micrograph picture at low magnification and (b) high-magnification SEM picture.

picture (Figure 5(a)). The deposition layers are delineated by bands of thin remelted nucleation zones formed at the layer interface. Extensively grown dendritic grains across a number of deposit layers (several millimeters) can also be seen occasionally. A high-magnification SEM picture in Figure 5(b) shows the detailed microstructure of the as-deposited material, where fine secondary dendrites are formed within a grain with an averaged dendrite arm spacing around 5 μm. In contrast to the dark austenite matrix, small white particles in globular and irregular shapes that have precipitated along the interdendritic boundaries can be seen. They are identified as the Laves phase and some minor MC and TiN phases that are segregated during the fast solidification process. Figure 6 shows the EDAX analysis on the major phases appearing in the as-deposited microstructure. Comparing Figures 6(b) and (c), one can observe that the matrix of the dendrite's core area is rich in Fe, Cr, and Ni, while the white segregation particles are rich in Nb, Mo, and Ti, which are the major compositional elements of the Laves phase.

Figure 7 shows the microstructure that went through a direct age heat treatment. Compared to the as-deposited microstructure, the direct-age treatment did not change the size of the dendrites and the morphology of interdendritic Laves phase. Elemental analysis by EDAX on the direct-aged matrix phase and

primary segregation phases shows similar results to the as-deposited phases, as shown in Figure 6. The aging temperatures are designed to precipitate γ'' and γ' strengthening phases in the γ matrix, but these temperatures are not high enough to dissolve the interdendritic Laves phase.

Figure 8 illustrates the microstructure after solution and aging heat treatment. As can be seen, most Laves phases have been transformed to needlelike structures (δ phase) at the interdendritic regions. Since the δ phase requires less Nb than the Laves phase, the transformation indicates that the as-deposited high concentration of Nb at interdendritic regions has been partially dissolved into the matrix after solution treatment. However, the solution temperature at 980 °C did not dissolve the Laves phase completely. It is found by EDAX that there are still occasionally some partially transformed Laves phase particles connecting with the δ-phase plates remaining in the interdendritic regions.

Figure 9 shows the microstructure that went through the complete homogenization (at 1093 °C) and STA heat treatment. As can be observed, the high temperature of homogenization results in considerable grain coarsening. Most Laves phase has been dissolved into the matrix and resulted in recrystallized large grains with bands of annealing twins. The primary MC and TiN phases, which appear in white small particles, are relatively stable phases and can still be found in the homogenized microstructure. The microstructure has a more isotropic appearance with recrystallized grains. As a result, one would expect more isotropic properties and increased ductility from this heat treatment. Figure 10 shows the EDAX elemental analysis results for the major phases after homogenization heat treatment, i.e., NbC particles, the remaining δ phase, and the matrix phase.

III. TENSILE PROPERTY TESTS

A. Test Sample Fabrication

Two types of deposition geometries were used for making the tensile specimens: (1) deposition of thin-walled geometry on the direct-aged wrought IN718 (DA718) coupon with the final size of 42 mm × 81 mm × 3 mm, as shown in Figures 11(a); and (2) fully deposited block with the size of 64 mm × 15 mm × 7 mm on stainless steel substrate (25 mm × 25 mm × 6 mm), as shown in Figure 11(b). The former sample is designed to represent the repair situations for compressor and blisk blades, where only direct-age heat treatment can be applied after repair. The strength of the interface between the deposited material and the wrought DA718 base material is evaluated in the tensile test. The base DA718 coupon was verified to have a microstructure consisting of fine equiaxed grains with a size of ASTM 11. The DA718 samples, as shown in Figure 11(a), were tested in two heat treatment conditions, i.e., as deposited and direct aged. No solution and homogenization heat treatments were applied to these samples due to the potential degradation risk to the
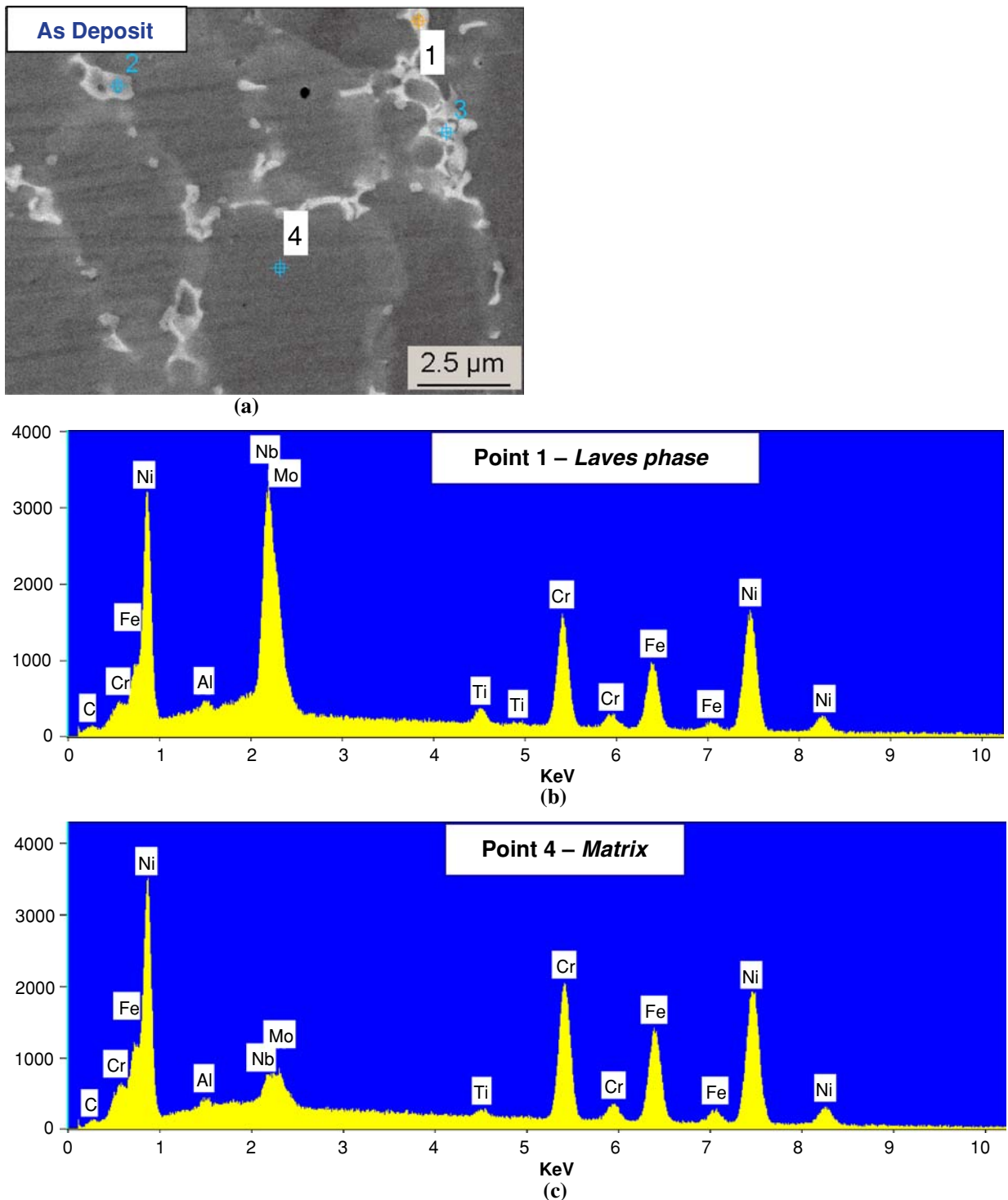
Fig. 6—EDAX elemental analysis on the major phases that appear in the as-deposited microstructure: (a) area of interest in SEM observation, (b) matrix elements, and (c) interdendritic Laves phase elements.

base material as a result of recrystallization and grain size coarsening. The fully deposited samples (Figure 11(b)) were divided into two groups and heat treated by standard STA and the homogenization STA method, respectively. The goal was to evaluate the laser deposition as a potential viable rapid manufacturing technique for new make parts. After

heat treatment, flat tensile bars 60.3 mm (L) × 12.7 mm (W) × 1.5 mm (T) that conformed to GE Aviation specifications were cut from the deposition samples by wire electrical discharge machining. For each heat treatment condition, two to four specimens were prepared and tested. All the tensile tests were conducted at room temperature.
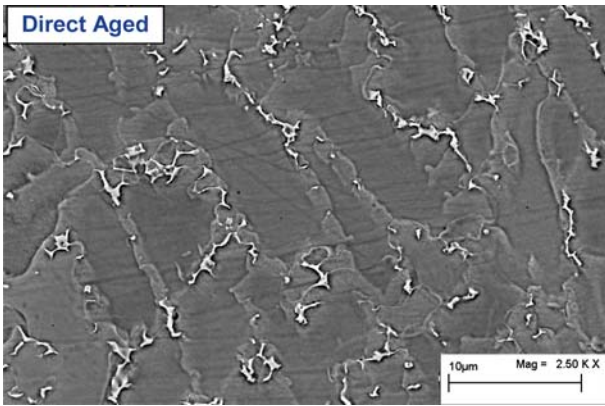
Fig. 7—Direct-aged microstructure shows similar dendrites and interdendritic phases as were seen in the as-deposited microstructure.
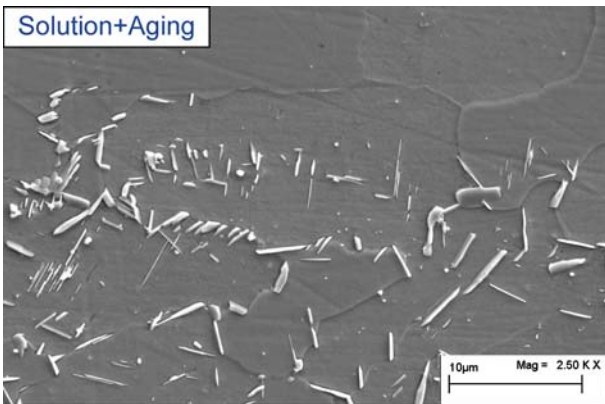

Fig. 8—Microstructure after solution and aging heat treatment shows most of the Laves phase has been transformed to needlelike δ phase at the interdendritic regions.
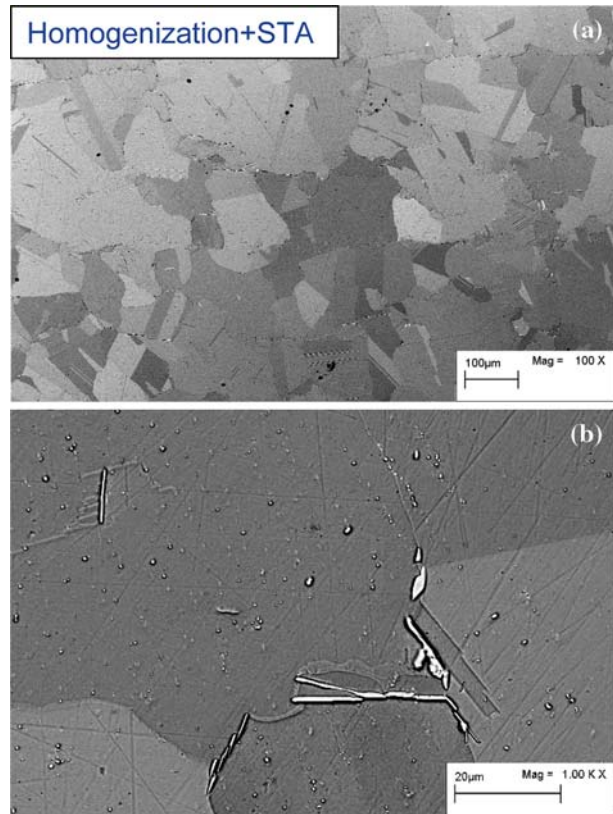

Fig. 9—Microstructure after the homogenization (at 1093 °C) and STA heat treatment shows (a) considerable grain growth with (b) occasional δ phase and MC phase at the grain boundaries.

B. Tensile Test Results

Figure 12 demonstrates the average ultimate stress, 0.2 pct yield stress, and plastic elongation of the tensile test results. These results were compared with different heat treatment conditions and the minimum properties from the AMS specifications for cast and wrought IN718, respectively. All the DA718 specimens (from Figure 11(a)) failed in the gage sections of the laser-deposited portions. The as-deposited material produces low yield stress (552 MPa) and ultimate stress (904 MPa) but relatively high plastic elongation (16.2 pct). After direct-age heat treatment, the ultimate stress increased by 47 pct to 1333 MPa, while the yield stress almost doubled and reached 1084 MPa. However, the plastic elongation of the direct-aged material compared with the as-deposited material dropped significantly from 16.2 to 8.4 pct. Although the direct-aged elongation value is still above the AMS cast property, it is much lower than the AMS wrought property, which is at 12 pct. The STA treatment condition produced slightly lower tensile strength (ultimate stress 1221 MPa) than wrought material, but it produced much better plastic elongation at 16.0 pct compared to the direct-aged condition. The material that underwent homogenization treatment produced slightly lower tensile strength (ultimate stress 1194 MPa) but even better elongation (19.9 pct) than the STA-treated material. In all cases, the heat-treated materials exhibited better tensile properties than the AMS cast properties but only marginally approached the wrought properties. Direct-aged tensile stress results were comparable to the wrought alloy, but they showed inferior ductility. The STA and homogenized STA treatments generated good ductility, which exceeded the minimum wrought elongation, but their tensile strength values were slightly below the wrought properties.

To compare the tensile behavior from different heat treatment conditions, one typical tensile test curve was chosen from each group of heat treatment specimens and plotted in Figure 13. Compared to the heat-treated materials, the as-deposited material was relatively soft and produced low yield and ultimate stresses, while demonstrating intermediate ductility. The heat-treated materials exhibited steeper elastic responses (higher modulus of elasticity) but yielded at different stress levels. The direct-aged curve yielded at the highest point followed by the STA curve and then the homogenization STA. After yielding, the three heat treatment conditions exhibited almost parallel stress-strain curves in the plastic elongation periods before necking. The direct age treatment improved the tensile strength of the
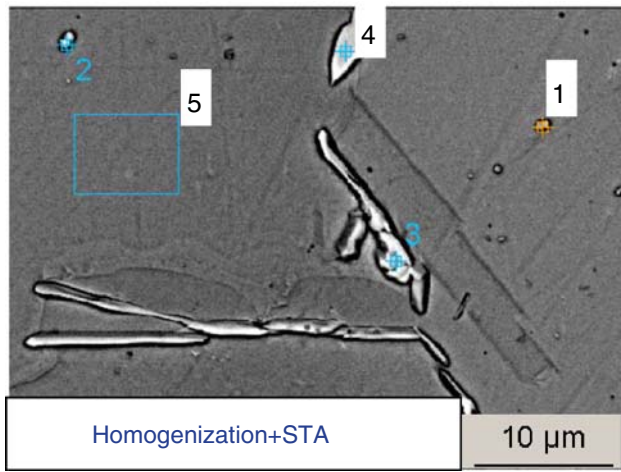
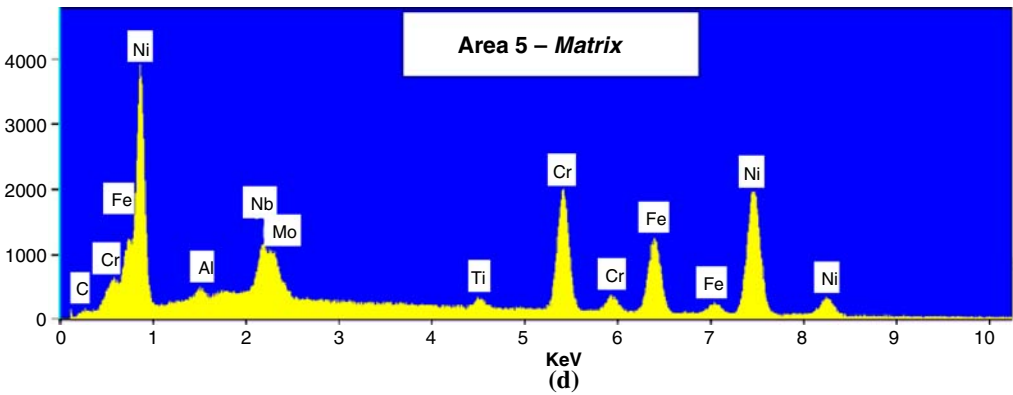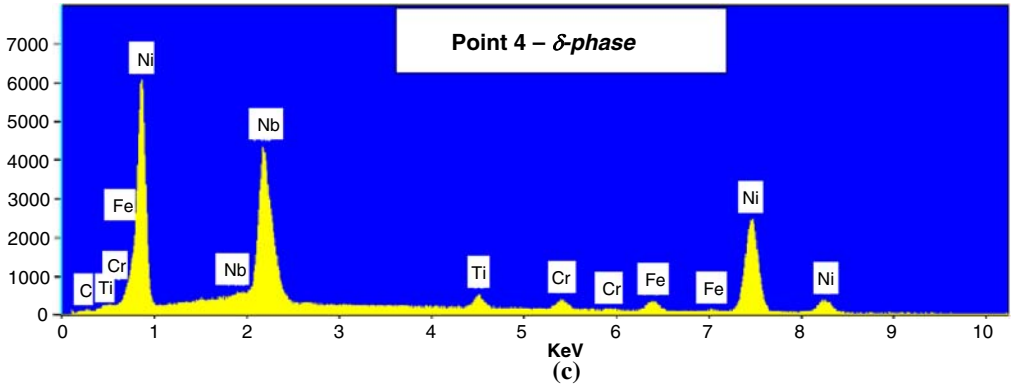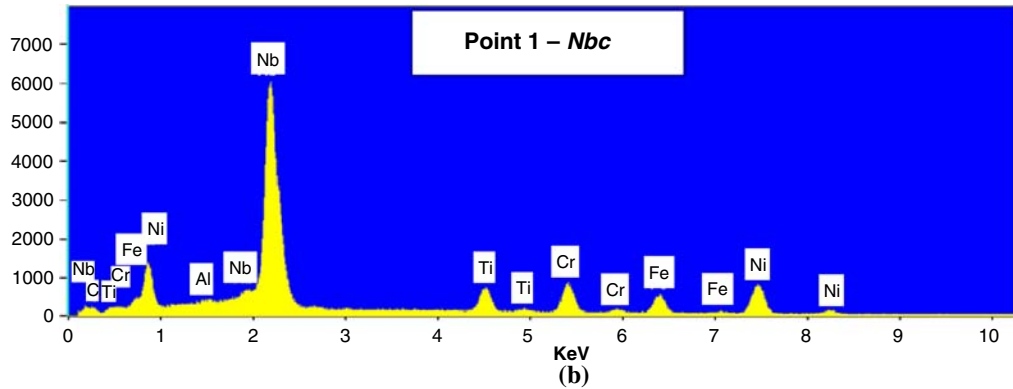Fig. 10—EDAX elemental analysis shows the major phases after homogenization heat treatment: (*a*) area of interest in SEM observation, (*b*) NbC phase, (*c*) δ phase, and (*d*) matrix phase.

deposit material substantially with a relatively short plastic elongation period. With the solution and age heat treatment, the plastic deformation curve was slightly lower than the direct-aged curve, but the ductility was significantly improved. When treated with a full cycle of homogenization, solution, and age, the 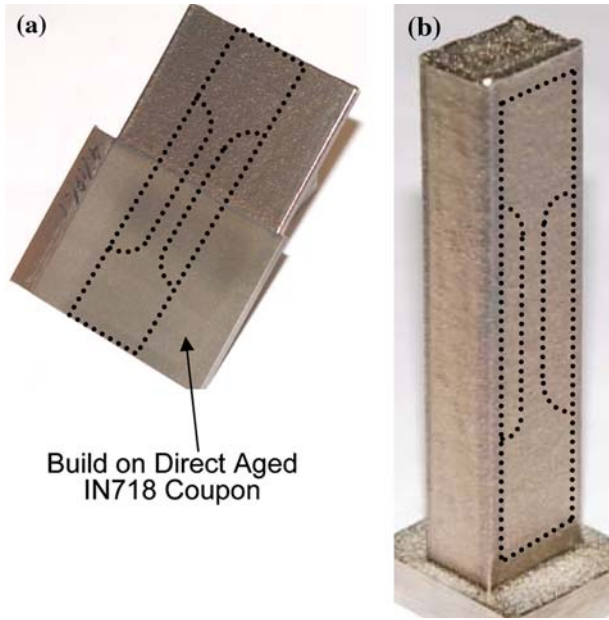material demonstrated extended plastic elongation before failure. This came at the cost of slightly lower yield and ultimate stresses.

The fracture surfaces of the tested specimens were examined under SEM. The as-deposited fracture surface exhibited a fine dimpled surface (Figure 14(a)), indicating a transgranular ductile mode of failure associated with good elongation. By contrast, the direct-aged fracture surface (Figure 14(b)) showed shallow dimples with protuberances composed of white particles, which are believed to be the Laves phase and MC carbides. This suggests the failure took place at the interdendritic regions or grain boundaries and was relatively brittle. Figure 15(a) shows the fracture surface of the STA heat-treated sample, which exhibits dendritic patterns with dimpled fracture features. This indicates that the fracture occurred preferentially along the interdendritic

Fig. 11—Tensile samples fabricated by laser powder deposition. (*a*) Thin-walled sample deposited on the wrought DA718 coupon for as-deposited and direct-age evaluations and (*b*) fully deposited block sample for STA and homogenization treatment evaluations.
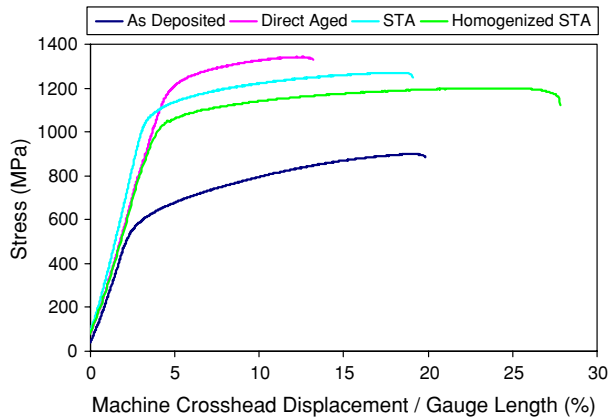

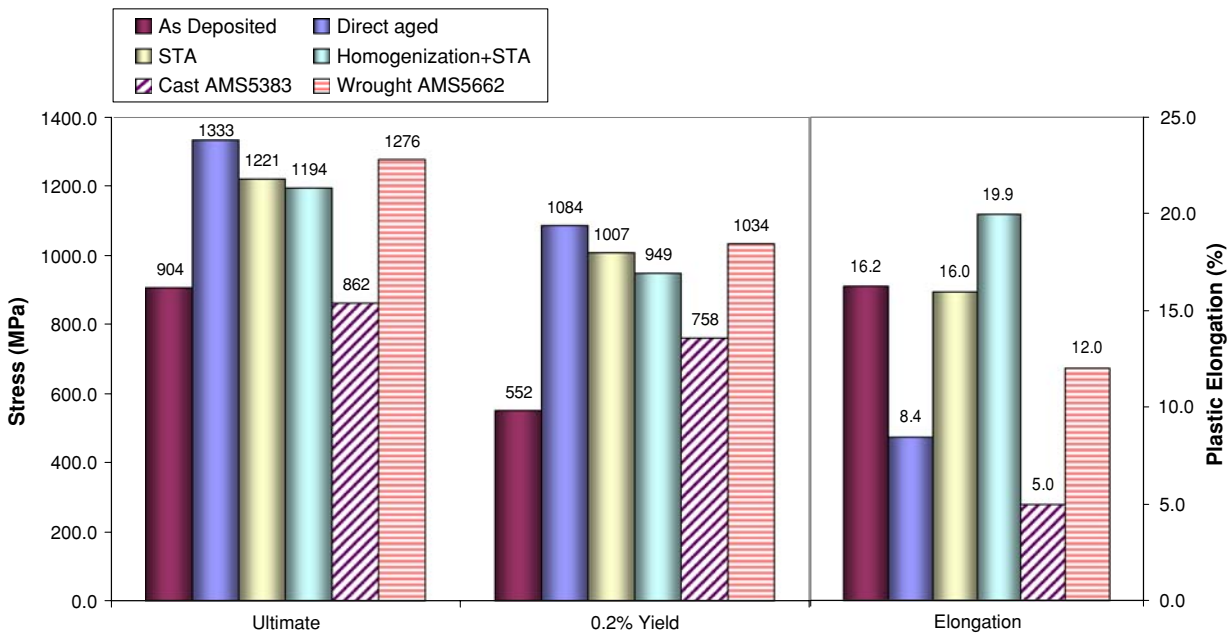Fig. 13—Tensile test curves comparing the different heat treatment conditions.

Fig. 12—Tensile test results showing the averaged ultimate stress, 0.2 pct yield stress, and plastic elongation compared with different heat treatment conditions and the AMS specifications for cast and wrought IN718, respectively.
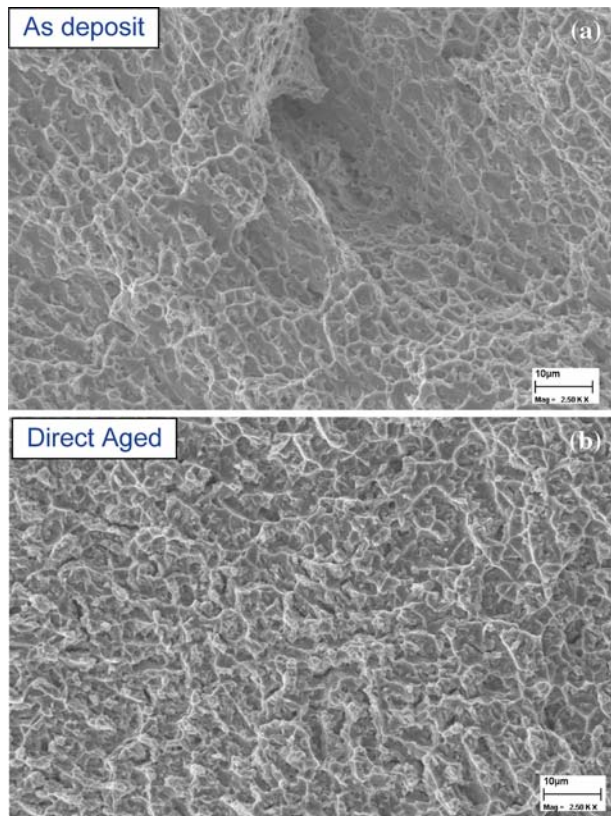
Fig. 14—Fracture surfaces of (*a*) the as-deposited sample and (*b*) the direct-aged sample.

Fig. 15—Fracture surfaces of (*a*) the STA-treated sample, (*b*) the homogenization, and the STA-treated sample.

regions and was a ductile failure. It was also observed that some white particles, *i.e.*, mostly δ phase and carbide particles, are present inside the dimples of the fracture surface, which suggests that these particles are the microvoid initiation sites associated with particle-matrix decohesion or particle fracture and eventually lead to the final transgranular fracture by void coalescence. In contrast to this, the fracture surface in the homogenized condition consisted of mostly fine shallow dimples and occasionally a few islands of flat surface areas approximately 100 μm in size. Figure 15(b) shows one such flat island in the fracture surface. This suggests that the failure has initiated from the relatively flat grain boundaries and propagated through coarsened grains, which were formed in the homogenization treatment.

IV. DISCUSSION

The microstructure of laser-deposited IN718 alloy exhibited various grain morphologies and size distributions. This was obviously caused by the dynamic heat transfer of the moving heat source and layered material formation mechanism. During laser deposition, material is built up layer by layer. When depositing a new layer of material, a thin top portion of the previous layer is remelted. As the molten pool solidifies, a thin nucleation zone at the layer interface is formed. As a result, layer boundaries consisting of fine grains can be observed,
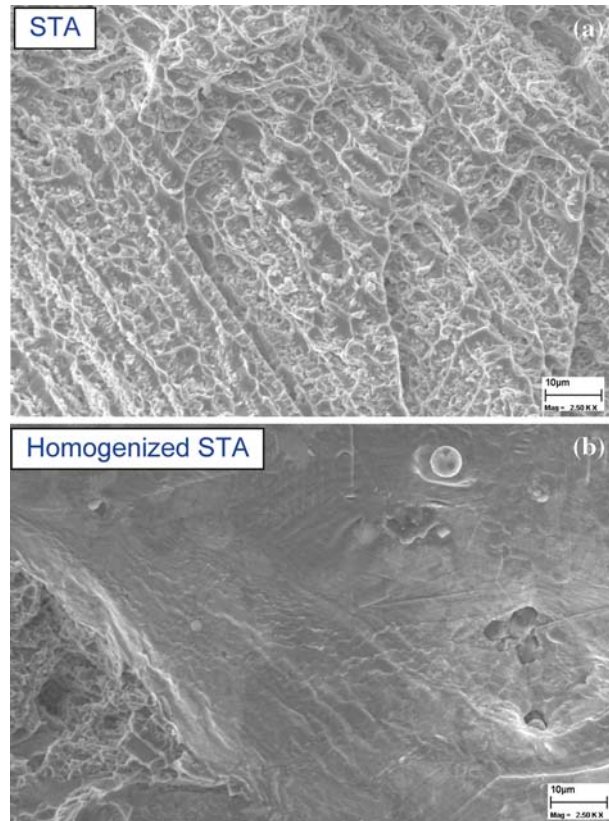
clearly delineating the deposit layers in the cross-sectional microstructure (Figure 5(a)). These layer interface regions are usually associated with sharp changes in grain size and degree of microsegregations; therefore, they can be the weak sites of tensile stress. Figure 16 compares the electron backscatter diffraction (EBSD)–generated grain/twin boundary overlay maps on the standard STA and homogenized STA microstructures, where the differences of grain morphologies and size distributions from the two heat treatments can be clearly seen. The layer interface regions can still be identified in the STA-treated material as bands of agglomerated fine grains (Figure 16(a)). This feature of layer boundaries disappeared in the homogenized microstructure, where the grains have been recrystallized and have a more isotropic appearance (Figure 16(b)). Figure 17 shows the microstructures of STA-treated material. It can be observed that bands of segregation-depleted regions are formed and also delineate the staggered deposition layers. It is also noticed that the edges of the deposit sample consist of relatively larger size grains (left areas in Figure 16(a)). This is a result of 30 pct higher energy input (high laser power and slower speed) used on the periphery contour of the rectangular sample in order to maintain good geometric accuracy. This portion of material was mostly removed during the preparation of tensile specimens; however, if the final specimen contained this microstructure, it may have contributed to deviations of the tensile properties.
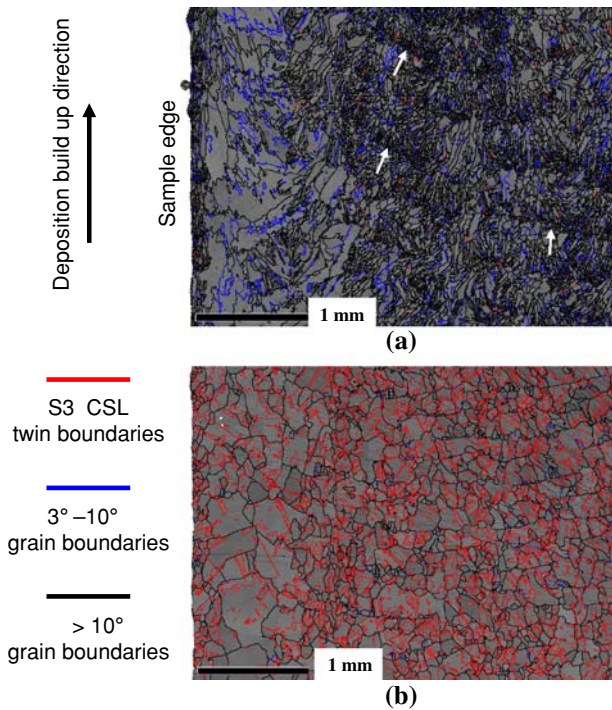
Fig. 16—Grain/twin boundaries overlay maps from EBSD analysis on (a) the standard STA-treated material (arrows pointing to the agglomerated fine grains at layer interfaces) and (b) the homogenization and STA-treated material.
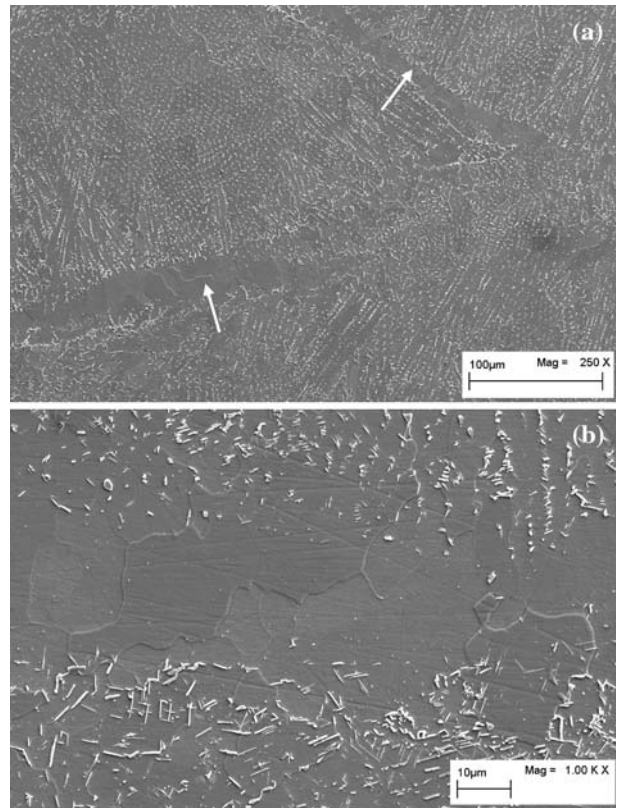

Fig. 17—Microstructure of STA-treated material showing bands of low Nb-rich segregation regions between the deposition layers (arrow pointed regions), which experienced grain growth during solution heat treatment.

The tensile test results have shown drastic strength changes from the as-deposited status to the direct-aged status. The cause for this is that the direct-aged heat treatment extensively precipitates fine γ'' and γ' strengthening phases in the matrix. These phases were suppressed during laser deposition because of the fast cooling rate. The Laves phase, in the form of fine particles along the interdendritic regions, was observed in both the as-deposited and the direct-aged microstructures with almost the same morphologies and volume fractions. It appears that the brittle Laves phase and carbide particles at the interdendritic regions, coupled with the fine γ'' and γ' precipitates in the matrix that lead to high tensile strength, are also responsible for the low ductility of the direct-aged material. Comparison of the tensile properties of the as-deposited material and the direct-aged material clearly indicates that the ductility of the material is closely related to the relative strength of the interdendritic phases and the matrix phases. The difference between the fractography pictures from the two conditions (Figure 14) indicates that once the matrix was strengthened by the γ'' and γ' precipitates, the brittle laves phase became the relatively weaker sites, initiating the fractures, and caused the reduced ductility of the material.

Standard STA heat treatment dissolved a good portion of the Laves phases and precipitated intergranular δ phase with acicular morphology. The literature has reported[4] that the Laves phase requires 10 to 12 pct Nb to form, the δ phase requires 6 to 8 pct Nb, the γ'' phase needs 4 pct Nb, and the γ' can form with Nb levels below 4 pct Nb. Too much of the Laves phase and δ-phase formation will deplete the available Nb for γ'' and γ' precipitation. The δ phase is an incoherent precipitate and does not contribute to alloy strengthening. Similar to the Laves phase, a large δ phase (Ni_3Nb) at grain boundaries is considered to associate with loss of strength for IN718;[12] however, the presence of δ phase at the grain boundaries has been reported to be beneficial for enhanced ductility and toughness.[13] This is because fine acicular δ phase at the grain boundaries provides an irregular morphology to the grain boundaries and thereby restricts grain boundary sliding and improves fracture ductility. Fine grain size is generally controlled during the wrought process using the appropriate δ solvus temperature.[4] A potential risk of the solution heat treatment is the nonuniformity of Nb concentration in the microstructure, because the δ solvus temperature is dependent on Nb concentration.[1] The required δ solvus temperature is decreased as the Nb content is decreased, and areas low in Nb will undergo recrystallization and grain growth during the solution heat treatment. The amount of Nb being rejected into the liquid pool from the solidification front is dependent on the temperature gradient and cooling rate along the molten pool boundary during deposition. Variations in these factors will exaggerate or deplete the Nb-rich segregation phases as well as change the grain size at the layer interface regions. During the period of

laser irradiation (laser spot size/scanning speed, on the order of 0.1 second), the high-temperature gradient and the slow cooling rate cause the formation of a thin Nb-depleted solidification layer. As soon as the laser beam moves away, the molten pool is quenched by the surrounding bulk material. The fast solidification speed is initiated and forms the microstructure with fine Nb-rich microsegregation, which is adjacent to the Nb-depleted layers. This microstructure after solution treatment will precipitate fine acicular δ phase at the Nb-rich regions, but it undergoes potential grain growth at the low Nb regions, as shown in the middle part of Figure 17(b). The nonuniformity of microsegregation at the deposition layer interface and the resultant grain size growth at low Nb regions during the STA heat treatment are probably the reason for slightly reduced tensile strength compared to the direct-aged material.

The homogenized STA has dissolved most of the Laves phase at the interdendritic regions; however, it has also caused substantial grain growth, as can be seen in Figures 9(a) and 16(b). The appearance of overwhelming twin boundaries, as shown in Figure 16(b), indicates the extended recrystallization from the homogenization treatment. There is very little δ phase precipitated after the subsequent solution treatment. As a result, recrystallized high-angle grain boundaries become long and prone to remain straight, which provides an easy path for crack propagation and notch brittleness. The SEM fractography observation also confirmed that the failure mode of the intergranular fracture was initiated from the large flat grain boundaries of the homogenized material. The standard 1093 °C/1 h homogenization treatment for cast material is probably overwhelming for the laser-deposited material and causes noticeable grain growth. As observed previously, segregation is not severe in the as-deposited microstructure, due to the fast cooling rate in the laser deposition process. Slightly lower homogenization and solution temperatures and shorter heating time are therefore recommended for the full treatment of the laser-deposited IN718.

V. CONCLUSIONS

This article studied the microstructure and tensile properties of IN718 alloy processed by the laser powder deposition process and the effects of post-heat-treatment methods that comply with the AMS standard specifications. The deposition process was optimized through a set of designed experiments to reduce the porosity caused by hollow powders and entrapped gas bubbles generated during the deposition process. It was found that the use of PREP powder or fine size (−200 mesh size) GA powder combined with a high laser deposition linear energy level (laser power/scanning speed) helps to reduce the porosity. Specifically, the deposit porosity was minimized to less than 0.03 pct when the PREP powder was used with a linear energy level greater than 80 J/mm.

The material microstructure and tensile properties of the laser-deposited IN718 alloy were studied and compared under the conditions of as deposit, direct age, solution treatment and age (STA), and homogenization followed by STA. It was found that the as-deposited alloy without any heat treatment remains soft and exhibits low tensile strength and good ductility (16.2 pct). The tensile strength was increased dramatically (100 pct improvement yield stress) and shown to be equivalent to wrought material after direct age due to the precipitation of the γ'' and γ' strengthening phases in the matrix; however, the ductility of the direct-aged material is reduced substantially to 8.4 pct due to fine Laves particles that remain at the interdendritic regions. These regions subsequently became relatively weaker sites, initiating fractures during tensile testing. Standard STA heat treatment has transformed most of the Laves phases to fine acicular δ phase at the interdendritic regions. Good ductility (16.0 pct) and slightly lower tensile strength (about 8 pct lower) were obtained from the STA treatment compared to the direct-aged condition. The low Nb bands formed at the deposit layer interfaces and the resultant grain size growth in these regions during the solution heat treatment seem to account for the slightly reduced tensile strength compared to the direct-aged material. The homogenized STA heat treatment completely dissolved the Laves phase but enabled substantial grain growth with isotropic appearance. As a result, this heat treatment produced the best ductility (19.9 pct), the tensile strength decreased 10 pct as compared to the direct-aged material.

REFERENCES

1. R.E. Schafrik, D.D. Ward, and J.R. Groh: in *Superalloys 718, 625, 706 and Various Derivatives*, E.A. Loria, ed., TMS, Warrendale, PA, 2001, pp. 1–11.
2. D.F. Paulonis and J.J. Schirra: in *Superalloys 718, 625, 706, and Various Derivatives*, E.A. Loria, ed., TMS, Warrendale, PA, 2001, pp. 13–23.
3. G.D. Janaki Ram, A. Venugopal Reddy, K. Prasad Rao, and G.M. Reddy: *Mater. Sci. Technol.*, 2005, vol. 21 (10), pp. 1132–38.
4. J.F. Radavich: in *Superalloys 718—Metallurgy and Applications*, E.A. Loria, ed., TMS, Warrendale, PA, 1989, pp. 229–40.
5. J.J. Schirra, R.H. Caless, and R.W. Hatala: *Superalloys 718, 625, and Various Derivatives*, TMS, Warrendale, PA, 1991, pp. 375–88.
6. G.D. Janaki Ram, A. Venugopal Reddy, K. Prasad Rao, G.M. Reddy, and J.K. Sarin Sundar: *J. Mater. Proc. Technol.*, 2005, vol. 167, pp. 73–82.
7. C.H. Radhakrishna and K. Prasad Rao: *J. Mater. Sci.*, 1997, vol. 32, pp. 1977–84.
8. P.L. Blackwell: *J. Mater. Process. Technol.*, 2005, vol. 170 (1–2), pp. 240–46.
9. I. Kelbassa, E.W. Kreutz, P. Albus, and L. Zhu: *Proc. 24th Int. Congr. on Applications of Lasers & Electro-Optics (ICALEO)*, Laser Institute of America, Orlando, FL, 2005, pp. 660–65.

10. X. Zhao, J. Chen, X. Lin, and W. Huang: *Mater. Sci. Eng. A*, 2008, vol. 478, pp. 119–24.
11. H. Qi, M. Azer, and P. Singh: *Int. J. Adv. Manuf. Technol.*, in press.
12. M.E. Mehl and J.C. Lippold: *Superalloys 718, 625, 706, and Various Derivatives*, TMS, Warrendale, PA, 1997, pp. 731–41.
13. G.A. Rao, M. Kumar, M. Srinivas, and D.S. Sarma: *Mater. Sci. Eng. A*, 2003, vol. 355, pp. 114–25.